*J. Fluid Mech.* (2009), *vol.* 638, *pp.* 401–421.  
doi:10.1017/S0022112009991108

# Nutrient transport and acquisition by diatom chains in a moving fluid

MAGDALENA M. MUSIELAK[1]†, LEE KARP-BOSS[2], PETER A. JUMARS[2] AND LISA J. FAUCI[3]

[1]Department of Mathematics, George Washington University, Washington, DC 20052, USA

[2]School of Marine Sciences, University of Maine, Orono, ME 04469, USA

[3]Department of Mathematics, Tulane University, New Orleans, LA 70118, USA

(Received 15 September 2008; revised 7 July 2009; accepted 7 July 2009; first published online 18 September 2009)

The role of fluid motion in delivery of nutrients to phytoplankton cells is a fundamental question in biological and chemical oceanography. In the study of mass transfer to phytoplankton, diatoms are of particular interest. They are non-motile, are often the most abundant components in aggregates and often form chains, so they are the ones expected to benefit most from enhancement of nutrient flux due to dissipating turbulence. Experimental data to test the contribution of advection to nutrient acquisition by phytoplankton are scarce, mainly because of the inability to visualize, record and thus imitate fluid motions in the vicinities of cells in natural flows. Laboratory experiments have most often used steady Couette flows to simulate the effects of turbulence on plankton. However, steady flow, producing spatially uniform shear, fails to capture the diffusion of momentum and vorticity, the essence of turbulence. Thus, numerical modelling plays an important role in the study of effects of fluid motion on diffusive and advective nutrient fluxes. In this paper we use the immersed boundary method to model the interaction of rigid and flexible diatom chains with the surrounding fluid and nutrients. We examine this interaction in two nutrient regimes, a uniform background concentration of nutrients, such as might be typical of an early spring bloom, and a contrasting scenario in which nutrients are supplied as small, randomly distributed pulses, as is more likely for oligotrophic seas and summer conditions in coastal and boreal seas. We also vary the length and flexibility of chains, as whether chains are straight or bent, rigid or flexible will affect their behaviour in the flow and hence their nutrient fluxes. The results of numerical experiments suggest that stiff chains consume more nutrients than solitary cells. Stiff chains also experience larger nutrient fluxes compared to flexible chains, and the nutrient uptake per cell increases with increasing stiffness of the chain, suggesting a major advantage of silica frustules in diatoms.

## 1. Introduction

The role that fluid motion plays in the transport of solutes to and away from micro-organisms suspended in oceans and lakes is a fundamental question in aquatic ecology, first addressed quantitatively by Munk & Riley (1952). Of particular interest is the transport of solutes to phytoplankton, the group of unicellular, photosynthetic

† Email address for correspondence: musielak@gwu.edu

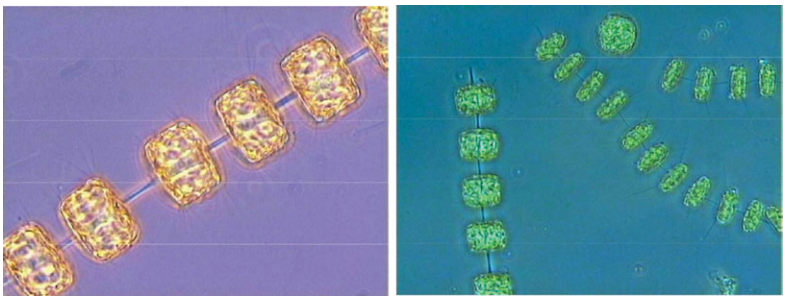

FIGURE 1. Chains of *Thallasiosira* from the Gulf of Maine. Photo courtesy of David Townsend, University of Maine.

micro-organisms that account for approximately 40 % of global annual primary production and are the foundation of aquatic food webs. Phytoplankton require dissolved nutrients (e.g. nitrate, phosphate, silicate, trace metals) for growth, and therefore processes that affect rates of nutrient delivery to cells may ultimately determine rates of primary production. Nutrients are delivered to the cell surface by molecular diffusion and then transported across the cell membrane via an enzymatically mediated uptake system.

A frequent misconception is that ambient flow can have no appreciable effect on nutrient fluxes and chemical boundary layer geometries at low Reynolds numbers. This misconception often arises from overzealous extrapolation of Purcell's (see Purcell 1977) classic assessment of 'Life at Low Reynolds Number' without sufficient attention to the fact that his focus was squarely on bacteria approximately 1 μm in diameter. Various approaches since the seminal assessment of Munk & Riley (1952), however, have indicated that when phytoplankton cells exceed a few tens of micrometres in radius, ambient fluid motion, as well as sinking and swimming, can enhance fluxes of solutes to or from cells (reviewed by Karp-Boss, Boss & Jumars 1996). Phytoplankton exhibit a wide range of cell, chain and colony sizes, from $<5$ μm to a few millimetres in length. At the upper end of these scales, ambient fluid motion, associated with dissipating turbulence, can enhance net diffusive fluxes by thinning diffusive chemical boundary layers that form around cells as a result of uptake (raise the Sherwood number). For simple shear flows and shapes, the extent of enhancement can be quantified through semi-empirical Péclet–Sherwood number relationships (Karp-Boss *et al.* 1996). In related low-Reynolds-number settings, Short *et al.* (2006) and Solari *et al.* (2006) demonstrated that flagellar stirring of boundary layers enhances nutrient uptake in colonies of volvocalean green algae.

Phytoplankton species for which ambient fluid motion can potentially become significant belong predominantly to the group of diatoms. This important group accounts for approximately half of total annual global phytoplankton production, and its members form intense spring blooms in coastal, temperate and high-latitude environments. Diatoms exhibit striking diversity of cell morphologies, and although unicellular, many species form chains and colonies (figure 1). A characteristic feature of diatom cells is encasement in a silica shell (called a frustule), with a consequent requirement for dissolved silicate, in addition to other nutrients.

It has been suggested that because phytoplankton are typically smaller than the Kolmogorov length scale in the ocean, the flow they experience is a linear shear flow (Lazier & Mann 1989). Thus, effects of turbulence on diatoms and other taxonomic groups of plankton have most often been simulated in steady Couette flows, with

various schemes for equating the steady shear produced with particular levels of turbulent dissipation (e.g. Shimeta, Jumars & Lessard 1995). In a steady Couette flow, phytoplankton cells that are elongate tend to align in the flow with their long axes parallel to the flow and tumble periodically (Jeffery 1922; Karp-Boss & Jumars 1998). Relative flow experienced by the cell during the tumble accounts for much of the flux enhancement in nutrient supply experienced by cells in a steady shear flow (Pahlow, Riebesell & Wolf-Gladrow 1997).

Steady flow, however, fails to capture the essence of turbulence. In steady Couette flow, there is no net diffusion of vorticity because it is spatially uniform with respect to shear. In decaying turbulence at the scales of phytoplankton there are gradients and therefore net diffusion of both momentum and vorticity, suggesting that tumbles may be much more prevalent, resulting in a more random distribution of orientations than seen in Couette flow (Jumars *et al.* 2009).

Numerical modelling has already played a significant role in understanding the role of relative fluid and particle motion in accounting for flux enhancement in nutrient uptake, specifically by identifying tumbling events as times of enhancement (Pahlow *et al.* 1997). Here we use a computational fluid dynamics approach to take three distinct steps towards greater realism in modelling of nutrient uptake by phytoplankton. First, we implement an unsteady shear flow to capture effects of unsteadiness. Second, we explicitly include flexural stiffness as a variable because phytoplankton form chains that vary in stiffness. Flexibility may enhance relative motion between cells and fluid when a chain that is flexed by fluid forces rebounds to its original shape. Third, we include two scenarios of nutrient distribution. For comparison with the bulk of past work, we include an initially uniform background concentration (that may be typical of high-nutrient conditions early in a spring bloom). We also simulate nutrient supply in more oligotrophic (chronically nutrient-poor) regions by providing randomly distributed point sources of nutrients (cf. Blackburn, Azam & Hagstrom 1997).

The actual dynamical system consisting of fluid, suspended phytoplankton chains and nutrient is obviously three-dimensional, as are the basic modelling equations described below. In order to calculate long-time temporal dynamics while varying parameters such as chain stiffnesses and background nutrient sources, the computations presented in this paper are two-dimensional. These two-dimensional simulations provide insight into this complex, coupled system and should be used as a starting point to distinguish among hypotheses and guide further investigation.

## 2. Mathematical model and numerical implementation

Because a goal of this model is to investigate effects of flexibility of diatom chains on nutrient acquisition, we choose an immersed boundary formulation (Peskin 2002; Mittal & Iaccarino 2005) that can readily capture the dynamic coupling of elastic structures with a viscous, incompressible fluid. The coupled system consisting of the fluid, the diatom chains and the nutrient is governed by the following equations in a rectangular periodic domain $\Omega$:

$$\rho\left(\frac{\partial \boldsymbol{u}}{\partial t} + \boldsymbol{u}\cdot\nabla\boldsymbol{u}\right) = -\nabla p + \mu\triangle\boldsymbol{u} + \boldsymbol{f}(\boldsymbol{x},t) + \boldsymbol{g}(\boldsymbol{x},t), \tag{2.1}$$

$$\nabla\cdot\boldsymbol{u} = 0, \tag{2.2}$$

$$\boldsymbol{f}(\boldsymbol{x},t) = \int_{\Gamma} \boldsymbol{F}(r,t)\delta(\boldsymbol{x} - \boldsymbol{X}(r,t))\,\mathrm{d}r, \tag{2.3}$$

$$\frac{\partial \boldsymbol{X}(r,t)}{\partial t} = \int_{\Omega} \boldsymbol{u}(\boldsymbol{x},t)\delta(\boldsymbol{x} - \boldsymbol{X}(r,t))\,\mathrm{d}\boldsymbol{x}, \tag{2.4}$$

$$\frac{\partial C}{\partial t} + \boldsymbol{u}\cdot\nabla C = \mathscr{D}\triangle C - R(\boldsymbol{x},C)\,C + S(\boldsymbol{x}). \tag{2.5}$$

Equations (2.1) and (2.2) are the incompressible Navier–Stokes equations, where $\boldsymbol{u}(\boldsymbol{x},t)$ is the fluid velocity, $p(\boldsymbol{x},t)$ is the pressure, $\boldsymbol{f}(\boldsymbol{x},t)$ is the force per unit volume exerted on the fluid by diatoms, $\boldsymbol{g}(\boldsymbol{x},t)$ is an external force that creates a background flow, $\rho$ is fluid density and $\mu$ is dynamic viscosity.

In our model the diatom chains are modelled as neutrally buoyant, elastic circles connected by filaments. The configuration of these immersed chains is defined by $\boldsymbol{X}(r,t)$, where $r$ is a Lagrangian label and $t$ is time. The force density $\boldsymbol{f}$ on the fluid domain in (2.3) is a delta-function layer whose source is the immersed chain $\Gamma$. The elastic forces $\boldsymbol{F}(r,t)$ generated along the passive diatom chain result by deformation from its equilibrium shape.

Equation (2.5) describes the diffusion, advection and reaction of nutrient concentration $C(\boldsymbol{x},t)$. Here $\mathscr{D}$ is its molecular diffusivity; $R(\boldsymbol{x},C)$ is the consumption rate; and $S(\boldsymbol{x})$ is a source. For simplicity, we assume that uptake by diatoms follows Michaelis–Menten kinetics, i.e. in the absence of spatial dependence

$$\frac{\mathrm{d}C}{\mathrm{d}t} = \frac{V_{max}}{C + K_m}\,C, \tag{2.6}$$

where $V_{\max}$ is the maximum uptake rate and $K_m$ is the half-saturation constant. We remark that while silicate uptake by diatoms has been shown to generally conform to Michaelis–Menten kinetics (Paasche 1973), more recent experiments indicate that non-saturable kinetics may occur for cells grown under silicon-replete conditions (Thamatrakoln & Hildebrand 2008).

In our model, cells act as moving sinks of nutrient, and we include a reaction term $R(\boldsymbol{x},C)\,C$. This is a localized function that is non-zero only at points distributed within the cells. Since the diatom chains are represented by Lagrangian points that move freely through the fluid domain, we use compactly supported smooth functions to transmit uptake from diatom cells to the fluid domain. Consequently,

$$R(\boldsymbol{x},C)\,C = \sum_{p=1}^{M_c} \int_{\Omega} \frac{V_{max}}{C_p + K_m}\,C_p\,\delta_{\beta}(\boldsymbol{x} - \widehat{\boldsymbol{X}}_{\boldsymbol{p}})\,\mathrm{d}\boldsymbol{x}, \tag{2.7}$$

where $M_c$ is the number of cells in the chain, $\widehat{\boldsymbol{X}}_{\boldsymbol{p}}$ is the centre of the $p$th cell and $C_p = C(\widehat{\boldsymbol{X}}_{\boldsymbol{p}}, t)$ is the nutrient concentration in the centre of the $p$th cell. The support $\beta$ of the bump function $\delta_{\beta}(\boldsymbol{x})$ depends on the radius of a cell and does not approach zero as numerical parameters are refined. The reaction term (2.7) allows us to keep track of the amount of nutrient taken up by each cell.

Diatom cell walls are permeated with tiny pores, that allow diffusion of nutrients and waste products in and out of the cell (Round, Crawford & Mann 1990). In our model nutrient may diffuse or be actively transported across the cell wall. However, cells and connecting filaments are not permeable to flow.

A background shear flow is achieved in our model in two ways. First, two neutrally buoyant, horizontal walls suspended within the fluid are moved in opposite directions to create a linear shear (see figure 2). These walls are also treated as immersed boundaries that generate forces due to stiff tether springs connecting material points of the walls to tether points whose motions are specified (Dillon *et al.* 1996). The speed

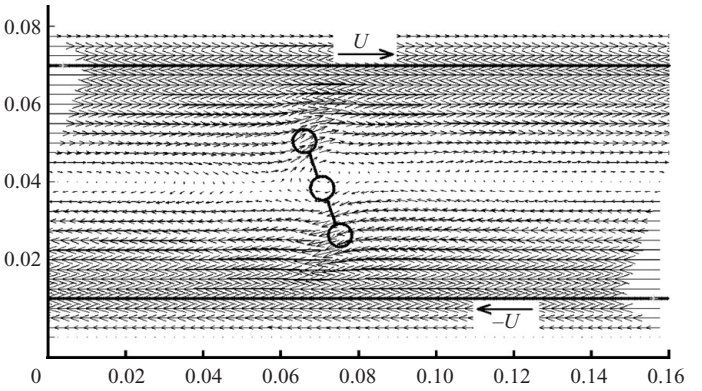


FIGURE 2. The two-dimensional flow field is created by the movement of the immersed horizontal walls, discretized on two horizontal lines. In the absence of the diatom chain, the flow would be a linear shear.

of these tether points is controlled to achieve a shear rate of $G = 0.5$–$1\ \mathrm{s}^{-1}$ (Karp-Boss *et al.* 1996). The second method we use to generate shear is to include a forcing term $\boldsymbol{g}(\boldsymbol{x}, t)$ in the Navier–Stokes equation (2.1) to create a vortical background flow.

### 2.1. *Representation of diatom chains*

We focus on *Thalassiosira* species that form flexible chains. Cells in a chain are joined by one or more threads extruded from a central, strutted process. As in all diatoms, their cell walls are rigid, made of biogenic silica (Werner 1977; Tomas 1997). Here, a diatom cell wall is modelled as a thin, neutrally buoyant band, which in the discrete representation is a collection of points located on a circle. Adjacent points on the circle are connected by linear springs. Also, to ensure that the shape of the cell is preserved throughout the simulation, we include linear springs that connect every second point on the circle. The stiffness constant of these springs making up the cell is $\sigma_S^C$. The thread is modelled as a thin band connecting two circles. In the discrete representation, the thread is a collection of points located on a curve, with adjacent points connected by elastic linear springs. The end points of the curve are also connected to the two circles by linear springs. The stiffness constant of these springs making up the threads is $\sigma_S^L$. The threads are initially straight, but depending on their flexibility, they change shape in time, as the diatom chain moves through the domain. This flexibility is controlled by bending-resistant forces along the thread that penalize departure from a straight configuration. The stiffness constant that dictates bending rigidity of the thread is $\sigma_B^L$. Bending-resistant forces are also applied along the cell wall with stiffness constant $\sigma_B^C$, but here the forces penalize deviation from the circular configuration. Similar immersed boundary forces were used in Fauci & McDonald (1994) to generate active bending motions of model flagella.

### 2.2. *Numerical implementation*

The continuum description of the governing equations of motion of the coupled fluid–diatom–nutrient immersed boundary system in (2.1)–(2.5) naturally suggests a time-stepping algorithm. At the beginning of each step we have the fluid velocity field $\boldsymbol{u}^n$, the locations of the immersed boundary points (walls and chains) $\boldsymbol{X}_l^n$ and the nutrient concentration field $C^n$. To advance the system by one time step we

(i) compute the immersed boundary force density $\boldsymbol{F}_l^n$;

(ii) spread the force density from immersed boundary to grid to get $\boldsymbol{f}_{i,j}^n$;

(iii) solve the Navier–Stokes equations for $\boldsymbol{u}_{i,j}^{n+1}$;
(iv) move the immersed boundary at the interpolated fluid velocity to get $\boldsymbol{X}_l^{n+1}$;
(v) use the updated positions of the cells to compute the nutrient uptakes;
(vi) solve the advection–diffusion–reaction equation for $C_{i,j}^{n+1}$.

The fluid domain $\Omega = [0, L_x] \times [0, L_y]$ is discretized, and the fluid variables are defined on a uniform Eulerian grid. The Navier–Stokes equations are solved in step (iii) above, using the projection method presented by Kim & Moin (1985). A second-order, explicit Adams–Bashforth scheme for the convective term is used, along with an implicit Crank–Nicolson treatment of the viscous terms.

The communication between Eulerian fluid quantities and Lagrangian immersed boundary quantities, in steps (ii) and (iv) above, uses a discrete approximation to the Dirac delta function. The same function is also used in modelling the sinks and sources on the nutrient concentration field. The two-dimensional discrete delta function is the product of two one-dimensional discrete delta functions $D_\beta(\boldsymbol{x}) = d_\beta(x)\, d_\beta(y)$, where $\beta = \beta(h)$ is the radius of $d_\beta$, that depends upon the grid spacing $h$. We choose $d_\beta$ with $\beta = 2h$ typically used in immersed boundary computations,

$$d_\beta(r) = \begin{cases} \dfrac{1}{2\beta}\left(1 + \cos\dfrac{\pi r}{\beta}\right) & \text{if } |r| < \beta, \\ 0 & \text{if } |r| \geqslant \beta. \end{cases} \tag{2.8}$$

To solve the nutrient transport equation (2.5) in step (vi) above, we use an implicit Crank–Nicolson scheme, with explicit treatment of the source and uptake terms. Uptake of nutrient by the cells replaces the function $\delta_\beta(\boldsymbol{x})$ appearing in (2.7) by the discrete approximation $D_\beta(\boldsymbol{x})$, but here the support $\beta$ is a physical parameter that does not depend on $h$, but on the radius of the cell, and is chosen so that the bump function $\delta_\beta$ covers about 75 % of the interior of the cell. Therefore, the reaction term $R(\boldsymbol{x}, C)\, C$ for the $p$th cell is discretized as

$$R_p^n = \sum_{i,j} \frac{V_{max}}{C_p^n + K_m}\, C_p^n\, D_\beta\left(\boldsymbol{x}_{i,j} - \widehat{\boldsymbol{X}}_{\boldsymbol{p}}^{\boldsymbol{n}}\right) h^2 \tag{2.9}$$

and gives the nutrient uptake rate by that cell in one time step. Throughout a simulation the uptake $R_p$ for each cell is calculated at every time step $n$ and is accumulated to give the total uptake of $\sum_n \triangle t\, R_p^n$.

Neumann boundary conditions for the nutrient concentration at the top and bottom walls are used when immersed boundary walls drive an unsteady shear flow, along with periodic boundary conditions at the sides. In other simulations, with no walls, we choose periodic boundary conditions for the nutrient concentration.

In Musielak (2007) we have presented convergence studies that demonstrate that our numerical solver has the desired accuracy; i.e. it is second order in both space and time in the absence of the immersed boundaries and first order when the immersed bodies are present.

To complete the description of our model, we have to specify the magnitudes of spring stiffness constants used in our simulations. As a starting point, our model assumes that cell walls are rigid everywhere, although limited data suggest that mechanical properties may not be uniform across the frustule (Almqvist *et al.* 2001). We are not aware of any measurements of elasticity of chains that we could incorporate in our models. Constants that keep all the circles in a chain rigid (deformations within 1 %) are found to be $\sigma_B^C = 10^{-5}\,\mathrm{g\,cm\,s^{-2}}$ and $\sigma_S^C = 200\,\mathrm{g\,cm^{-1}\,s^{-2}}$.

| Parameter | Numerical value |
|---|---|
| Time step | $\Delta t = 0.00015625$ s |
| In case of linear shear: | |
| Fluid domain size | $L_x \times L_y = 0.16 \times 0.08$ cm |
| Grid size | $N \times M = 256 \times 128$ |
| Nutrient domain size | $L_x^N \times L_y^N = 0.16 \times 0.06$ cm |
| Grid size | $N \times P = 256 \times 97$ |
| In case of vortical flow: | |
| Fluid/nutrient domain size | $L_x \times L_y = 0.4 \times 0.4$ cm |
| Grid size | $N \times M = 256 \times 256$ |
| Stiffness constants on circles: | |
| Stretching | $\sigma_S^C = 200\,\mathrm{g\,cm^{-1}\,s^{-2}}$ |
| Bending | $\sigma_B^C = 10^{-5}\,\mathrm{g\,cm\,s^{-2}}$ |
| Stiffness constants on connecting bands: | |
| Stretching | $\sigma_S^L = 90\,\mathrm{g\,cm^{-1}\,s^{-2}}$ |
| Bending | $\sigma_B^L = 10^{-7}$–$10^{-4}\,\mathrm{g\,cm\,s^{-2}}$ |

TABLE 1. Numerical parameters used in our model.

The bands that connect the cells may be rigid or flexible but should be nearly inextensible. We find that $\sigma_S^L = 90\,\mathrm{g\,cm^{-1}\,s^{-2}}$ keeps the chain within 2 % of its resting length (Musielak 2007). Finally, flexibility of the chains is controlled by the bending stiffness constant on the connecting bands, which we vary from $\sigma_B^L = 10^{-7}\,\mathrm{g\,cm\,s^{-2}}$ to $\sigma_B^L = 10^{-4}\,\mathrm{g\,cm\,s^{-2}}$. Other numerical parameters and all stiffness constants are shown in table 1.

Flow parameters in the model were set to represent expected values of shear rate and steadiness in the upper mixed layer in the ocean. The steadiness of the shear can be estimated from the Kolmogorov time scale of the smallest velocity fluctuation associated with dissipating Kolmogorov-scale eddies in the ocean (Tennekes & Lumley 1972; Karp-Boss & Jumars 1998),

$$\tau = 2\pi\left(\frac{\nu}{\varepsilon}\right)^{1/2}, \tag{2.10}$$

where $\varepsilon$ is the kinetic energy dissipation rate and $\nu$ is the kinematic viscosity. Oceanic values of the kinetic energy dissipation rate range from about $10^{-6}\,\mathrm{cm^2\,s^{-3}}$ in the deep ocean to $10^{3}\,\mathrm{cm^2\,s^{-3}}$ in regions of strong turbulence (e.g. the surf zone) (Thorpe 2007). The time scales of the smallest velocity fluctuations of flow in the ocean range from about 6 to 200 s. We can determine the time scale for a given shear rate $G$ using the fact that the energy dissipation rate $\varepsilon$ is proportional to the shear of the turbulent velocity field, i.e.

$$\varepsilon \approx \nu\left(\frac{\partial u}{\partial x}\right)^2, \tag{2.11}$$

which gives

$$G \approx \left(\frac{\varepsilon}{\nu}\right)^{1/2}. \tag{2.12}$$

For the measured values of energy dissipation rates, $\varepsilon = 2.5 \times 10^{-3}\,\mathrm{cm^2\,s^{-3}}$ to $\varepsilon = 1.0 \times 10^{-2}\,\mathrm{cm^2\,s^{-3}}$, the expected shear rate is $G = 0.5$–$1\ \mathrm{s^{-1}}$ (Karp-Boss *et al.* 1996). For

| Characteristic quantity | Symbol | Value |
|---|---|---|
| Characteristic length (cell radius) | | |
| In linear shear | $L$ | $3.0 \times 10^{-3}$ cm |
| In vortical flow | | $6.5 \times 10^{-3}$ cm |
| Characteristic velocity (maximum velocity) | | |
| In linear shear | $U$ | $1.5 \times 10^{-2}$ to $3.0 \times 10^{-2}$ cm s$^{-1}$ |
| In vortical flow | | $6.5 \times 10^{-2}$ cm s$^{-1}$ |
| Fluid density | $\rho$ | 1 g cm$^{-3}$ |
| Fluid viscosity | $\mu$ | $10^{-2}$ g cm$^{-1}$ s$^{-1}$ |
| Diffusivity | $\mathscr{D}$ | $10^{-5}$ cm$^2$ s$^{-1}$ |
| Kinetic energy dissipation | $\varepsilon$ | $2.5 \times 10^{-3}$ to $1.0 \times 10^{-2}$ cm$^2$ s$^{-3}$ |
| Shear rate | $G$ | 0.5–1.0 s$^{-1}$ |
| Maximum uptake rate | $V_{max}$ | 0.1395 nmol cm$^{-3}$ s$^{-1}$ |
| Half-saturation constant | $K_m$ | 2.27 nmol cm$^{-3}$ |
| Reynolds number | $Re$ | $4.5 \times 10^{-3} - 4.2 \times 10^{-2}$ |
| Péclet number | $Pe$ | 4.5–42 |
| Kolmogorov time scale | $\tau$ | 6–13 s |

TABLE 2. Characteristic physical parameters governing diatom–nutrient system. Magnitudes of $V_{max}$, $K_m$ from Martin-Jézéquel, Hildebrand & Brzezinski (2000) are given for silicon uptake by diatoms.

that shear rate, the time scale of the smallest turbulent fluctuations is of the order of 6–13 s, and flow can be considered steady over shorter periods.

To keep our simulations consistent with the above scales, we move the walls of our model with speeds that create a shear rate $G = 0.5$–$1$ s$^{-1}$, and we change direction of their movement every 6–13 s. In case of the vortical background flow generated by the force $\boldsymbol{g}(\boldsymbol{x}, t)$ we shift the position of the vortices every 6–13 s to stay consistent with the time scale of the smallest velocity fluctuations. All the characteristic physical quantities are listed in table 2.

## 3. Numerical results

### 3.1. *Nutrient uptakes*

In all the simulations with shear flow in a channel, each cell in a chain has a 30 μm radius, and connections between cells are 70 μm long. The top and bottom walls are moved in opposite directions at constant velocity.

We first consider the case in which the spatial concentration of nutrient is initially uniform, and we keep track of nutrient uptakes by cells in chains of different flexibilities. We start with the top wall moving to the right and the bottom wall moving to the left, for 8 s. Both walls are then stopped for 1 s, after which the direction of their movement is reversed. This oscillating motion of walls is continued for the rest of the simulation. Cells in the flexible chain stay close together most of the time, and the chain rotates slower. The stiffer chain, on the other hand, rotates more rapidly, and cells stay apart from each other, thus maintaining larger effective size (figure 3). In this situation, under nutrient-replete conditions, the difference in nutrient consumption between chains of different flexibilities is very small. At the end of the

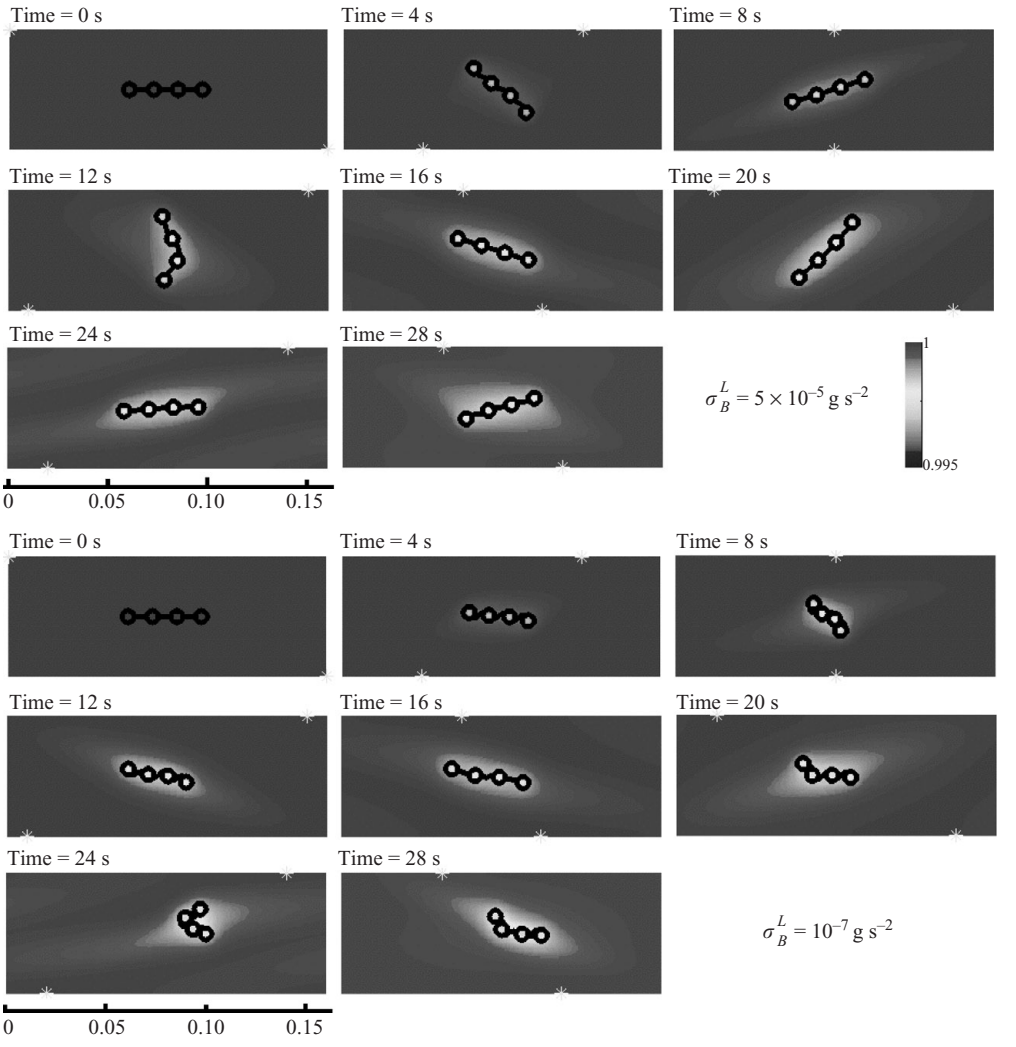


FIGURE 3. Evolution of nutrient concentration and position of diatom chains in an oscillating shear flow. The chain in bottom frames is more flexible than the chain in top frames.

simulation, the uptake by the stiff chain is larger by less than 0.05 %. Differences in uptake between solitary cells and cells arranged in chains are also insignificant.

One can estimate from the first three snapshots in figure 3 that the period of half rotation of the stiffer chain is approximately 10 s. This is about half of the period predicted by Jeffery's theory for a rigid ellipsoid with axis ratio $r_a = 7.5$ (Jeffery 1922), which is the length of the straight chain divided by the diameter of a cell. Of course, Jeffery's theory is not directly applicable, since here the fluid dynamics is two-dimensional, and the chain is not a rigid ellipsoid. Periods of rotation of *Thalassiosira* measured by Karp-Boss & Jumars (1998) in a steady shear flow ($G = 0.5{-}1$ s$^{-1}$) were 0.3–0.8 times those predicted by Jeffery's theory.

We next consider zero initial distribution of nutrient, with patches of it appearing randomly in the channel throughout the simulation. We run a set of experiments on chains of three, four and five cells, with varying flexibility. Initially chains are placed

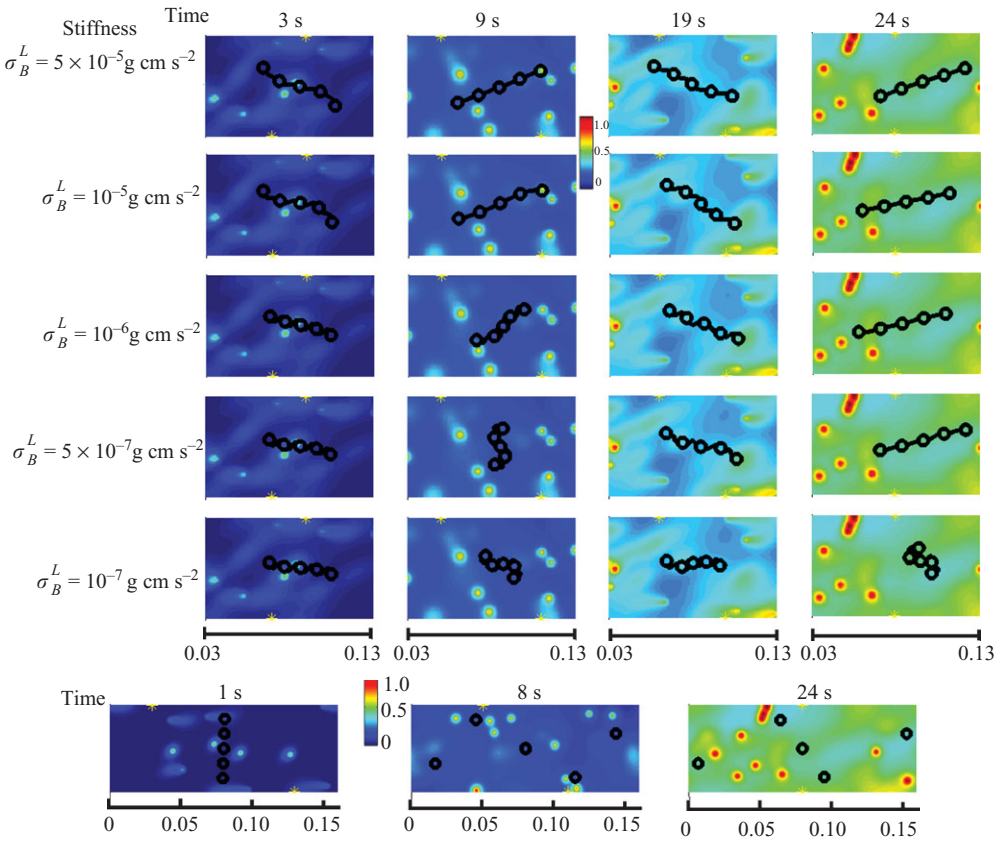


FIGURE 4. Evolution of nutrient concentration and position of diatom chains in an oscillating shear flow. The flexibility of chains increases from top to bottom in the first five set of frames. The last three frames show snapshots of solitary cells immersed in the same flow.

in the middle of the channel at a nearly horizontal position. The walls are moved in opposite directions, and stop every 6–7 s for 1–2 s, and then change directions. This oscillating shear flow is consistent with Kolmogorov time scales in the ocean. Nutrient patches appear every second in 10 random places throughout the channel, and the sequence is the same for each set of simulations with chains of equal length (figure 4). We also perform simulations with solitary cells, to determine whether there is any advantage for cells to stay connected in a chain.

To quantify the relation between nutrient uptake and flexibility of chains, we calculate the differences in nutrient uptakes per cell between every chain of a given flexibility, as a function of time, relative to the consumption by the most flexible chain ($\sigma_B^L = 10^{-7}$ g cm s$^{-2}$). The results suggest that nutrient uptake per cell increases with increasing stiffness of the chain (figure 5*a*). The difference in uptake between the most flexible and the stiffest chain of three cells reaches 9 %. Similar results were seen in experiments with chains of four and five cells.

In the same way we compare the uptake per cell by chains to consumption by solitary cells. The differences for chains of three cells relative to the uptake by solitary cells are shown in figure 5(*b*) and for chains of five cells in figure 6. From these, and from similar results with chains of four, it appears that cells arranged in stiffer chains

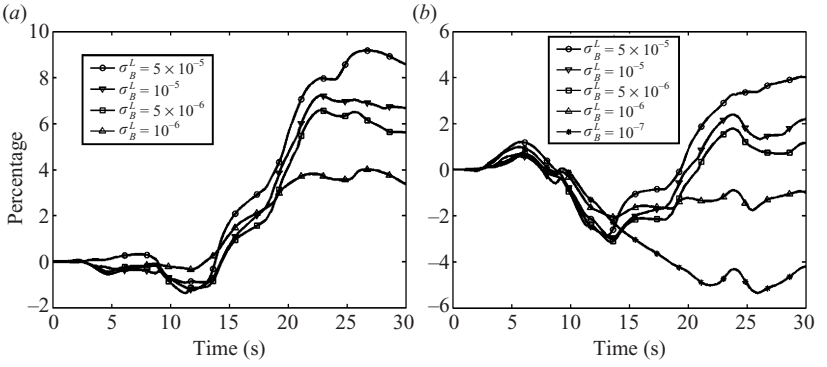


FIGURE 5. (*a*) Differences in nutrient uptake by every chain of three cells and the most flexible chain ($\sigma_B^L = 10^{-7}$ g cm s$^{-2}$), relative to the uptake by most flexible chain. (*b*) Differences in uptakes by chains of three cells and solitary cells, relative to the uptake by solitary cells.

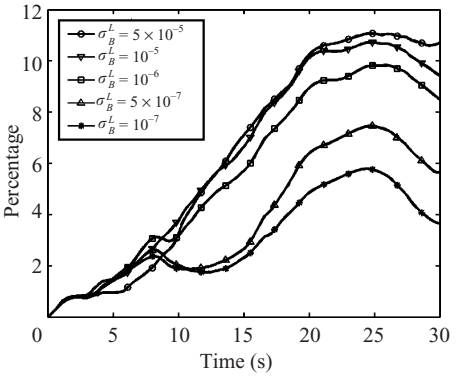


FIGURE 6. Differences in uptakes by chains of five cells and solitary cells, relative to the uptake by solitary cells.

are able to consume more nutrient in these flows than cells that are not arranged in chains.

In order to further investigate the relation between patch distributions and uptake differences between chains of varying flexibility, we performed a set of experiments in which the spatial and temporal distributions of nutrient sources were varied systematically, considering only chains of five cells. Using the previous set-up as our baseline (10 patches every second), we first keep the number of patches constant but decrease the frequency with which they appear in the channel, down to 10 patches every 2 and 4 s. Next, we keep the frequency constant but double and halve the number of patches that appear in the channel every second. The differences in uptakes between a given chain and the most flexible chain with the same nutrient patch history are normalized by the uptake by the most flexible chain. These ratios are presented in table 3.

When twice the number of patches are introduced into the channel, the differences in uptake get significantly smaller, e.g. from 6.7 % down to 1.6 % for the stiffest chain. Note that doubling the number of patches brings the results closer to nutrient-replete conditions, where we measured very small differences in uptake. Cutting the frequency of patch introduction in half, from 1 to 2 s, slightly increases differences in uptake.

| $\sigma_B^L$ (g cm s$^{-2}$) | 1 s | 2 s | 4 s | 5 patches | 20 patches |
|---|---|---|---|---|---|
| $5 \times 10^{-5}$ | 6.7 | 8.1 | 8.6 | 5.8 | 1.6 |
| $10^{-5}$ | 5.6 | 7.4 | 5.2 | 3.7 | 1.3 |
| $10^{-6}$ | 4.7 | 5.3 | 3.3 | 4.4 | 0.7 |
| $5 \times 10^{-7}$ | 2.0 | 3.8 | 1.0 | 3.1 | −0.6 |

TABLE 3. Differences in nutrient uptake (in per cent), relative to uptake by chains with $\sigma_B^L = 10^{-7}$ g cm s$^{-2}$, calculated at the end of simulations. Results in the first column (1 s) correspond to figure 6. The second and third columns correspond to 10 patches of nutrient introduced into the channel every 2 and 4 s, respectively. The last two columns show results from simulations in which 5 and 20 patches of nutrient are introduced every second.

But decreasing frequency even more does not produce even larger differences. In all simulations, it is the stiffest chain that enjoys the largest nutrient uptake. Cells in flexible chains tend to stay close together, and they also rotate slower. In stiffer chains, on the other hand, cells stay apart from each other, rotate more rapidly and cover more territory, thereby increasing chances of encountering more nutrient patches.

### 3.2. *Nutrient fluxes*

#### 3.2.1. *Diffusive boundary layer and Sherwood number*

We return to the study of the relation between flexibility of chains and nutrient acquisition under replete nutrients. Instead of measuring nutrient uptakes we concentrate on nutrient fluxes and examine the effect of fluid motion on nutrient flux. To quantify enhancement of fluxes towards the cell due to advection, we calculate the Sherwood number. It indicates how many times more flux occurs across the surface of a cell in the presence of fluid motion than in its absence and is used to study effects of different processes on convective and diffusive mass transport. Simulations that keep track of fluid velocity fields and chemical fields allow computation of local and time-dependent Sherwood numbers (Kiørboe, Ploug & Thygesen 2001; Kleis & Rivera-Solorio 2003; Tada & Tarbell 2004; Li, Deen & Kuipers 2005).

In the absence of fluid motion, the concentration distribution of a nutrient $C$ about a planktonic cell is given by the diffusion equation. In an idealized situation of a spherical organism sitting motionless in a motionless ocean, diffusion is radial. In two dimensions the solution of the steady-state diffusion equation is

$$C(r) = A \ln r + B. \tag{3.1}$$

If the concentration at the cell surface, i.e. at $r = R$, is $C_0$, and the concentration at the far-field $r = R_\infty$ is $C_\infty$, then (3.1) becomes

$$C(r) = \frac{C_\infty - C_0}{\ln \frac{R_\infty}{R}} \ln \frac{r}{R_\infty} + C_\infty. \tag{3.2}$$

When uptake capacity of the cell exceeds diffusional supply rate, there exists a nutrient-depleted region in the vicinity of the cell. This region is called 'the diffusive boundary layer' (DBL) and is commonly defined as the region in which the difference between $C$ and $C_0$ is less than 90 % of $(C_\infty - C_0)$ (Karp-Boss *et al.* 1996). The size of the DBL will depend on both $R$ and $R_\infty$, and in the idealized situation it will extend to $r = (R/R_\infty)^{0.1} R_\infty$ away from the cell centre. In shear flow, the boundary layer will be distorted, and the concentration gradients will steepen in certain regions.

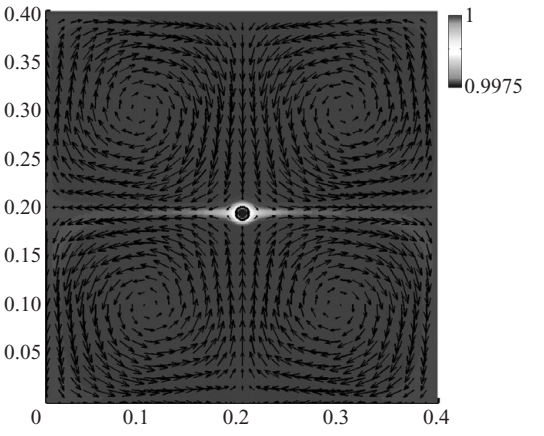


FIGURE 7. Nutrient concentration distribution and the velocity field after 30 s.

The Sherwood number for a cylindrical cell is given by

$$Sh = \frac{-\int_0^{2\pi} \frac{\mathrm{d}C}{\mathrm{d}r} R \, \mathrm{d}\theta}{\int_0^{2\pi} \frac{(C_0 - C_\infty)}{\ln \frac{R_\infty}{R}} \mathrm{d}\theta} = \frac{-R \ln \frac{R_\infty}{R} \int_0^{2\pi} \frac{\mathrm{d}C}{\mathrm{d}r} \, \mathrm{d}\theta}{2\pi(C_0 - C_\infty)}. \tag{3.3}$$

Notice that in the case of a cylindrical cell in a stagnant fluid $Sh = 1$, and as the thickness of the DBL decreases due to flow in the vicinity of the cell, the Sherwood number increases.

To ensure a well-defined far-field concentration $C_\infty$, used in calculating the Sherwood number, we enlarge our domain and create the background flow not with the walls used in previous experiments but by applying the following forcing term in the Navier–Stokes equations:

$$\boldsymbol{g}(\boldsymbol{x}, t) = \left( \rho a^2 \sin\left(\frac{2\pi}{L_x} x - s_x\right) \cos\left(\frac{2\pi}{L_x} x - s_x\right) + 2a\mu \sin\left(\frac{2\pi}{L_x} x - s_x\right) \cos\left(\frac{2\pi}{L_y} y - s_y\right), \right.$$
$$\left. \rho a^2 \sin\left(\frac{2\pi}{L_y} y - s_y\right) \cos\left(\frac{2\pi}{L_y} y - s_y\right) - 2a\mu \cos\left(\frac{2\pi}{L_x} x - s_x\right) \sin\left(\frac{2\pi}{L_y} y - s_y\right) \right),$$

where $L_x \times L_y$ is the size of the domain. The magnitude and sign of the parameter $a$ determine the strength and direction of the flow, and parameters $s_x, s_y$ are used to shift positions of vortices.

The boundary conditions for nutrient concentration are periodic in all directions; the initial distribution is uniform; and the domain is big enough (relative to the cell size) that the uptake of the cells cannot influence the far-field $C_\infty$ in the time under consideration. Our domain is chosen to be $0.4 \times 0.4$ cm, to be consistent with the length scale of dissipative eddies in the ocean (Jumars *et al.* 2009), making the vortices 0.2 cm in diameter. Each cell in our simulations has the radius of 65 μm.

### 3.2.2. *Solitary cell*

Before studying the effects of fluid motion on nutrient fluxes for chains, we first examine the behaviour of the Sherwood number for a single cell. We perform two experiments. First we put a single cell at a stagnation point in the middle of the domain and impose vortical background flow (figure 7). We expect that the cell will

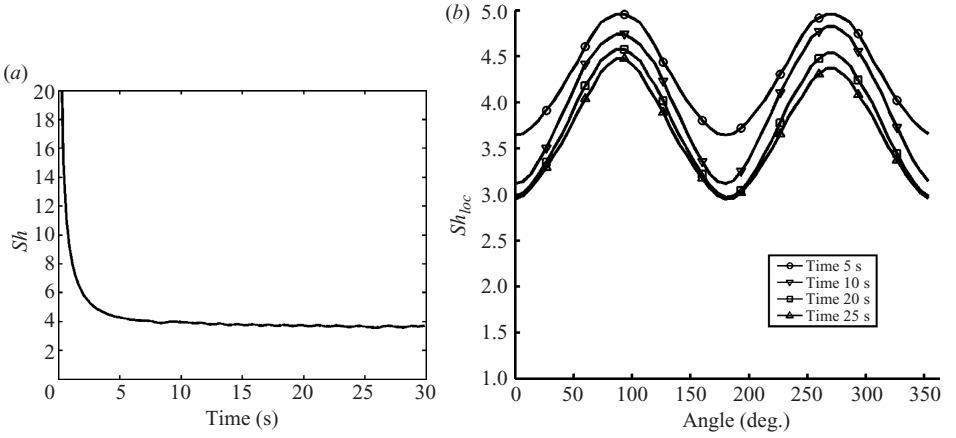


FIGURE 8. (*a*) Evolution in time of the overall Sherwood number for the cell and (*b*) the local Sherwood number ($Sh_{loc}$) along the perimeter of the cell; zero angle is at '9 o'clock' and increases counterclockwise.

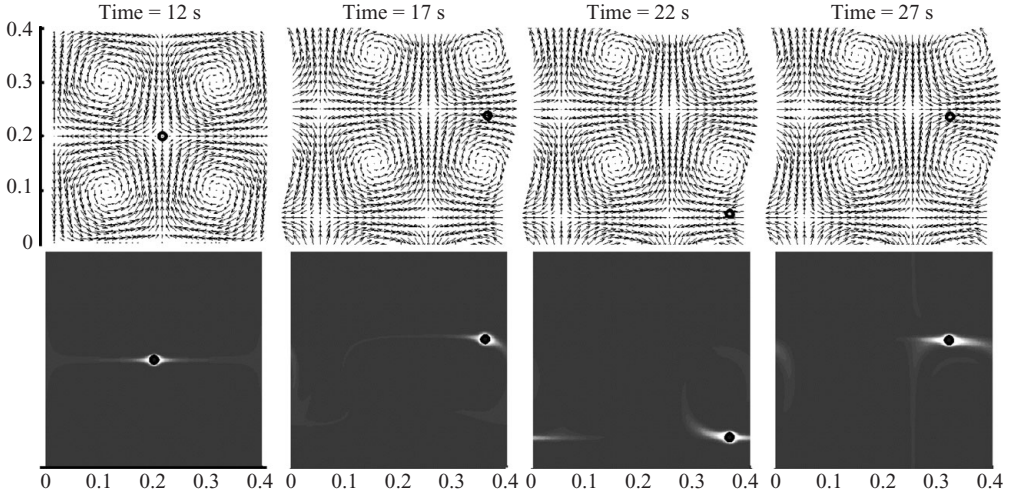


FIGURE 9. Snapshots of the nutrient concentration distribution, the position of the cell and the velocity field throughout the simulation.

experience a large enhancement of flux because of the oncoming flow. Due to the flow, the DBL around the cell is distorted, and concentration gradients steepen in certain regions, which is reflected in the local Sherwood number (figure 8*b*). In the areas of oncoming flow, the local Sherwood number increases, and where the DBL thickens the local Sherwood number decreases. The overall Sherwood number for the cell is initially large because the difference between $C_\infty$ and $C_0$ is small. That behaviour of *Sh* was also observed by Kleis & Rivera-Solorio (2003) in their study of unsteady mass transfer from a sphere in a non-uniform concentration distribution. In our simulation *Sh* quickly goes down to the value of approximately 3.8 (figure 8*a*).

In the second experiment, we again put a single cell in the middle of the domain and impose the vortical background flow, but after 14 s we change the position of the vortices ($s_x = s_y = \pi/4$), so that the cell starts moving with the flow (figure 9). While the cell stays at the stagnation point the Sherwood number is about 3.8, but

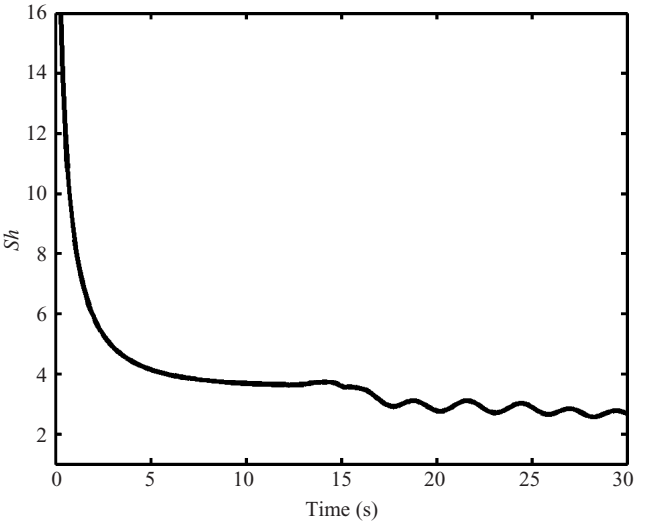


FIGURE 10. Evolution in time of the overall Sherwood number for the cell.

as the cell starts moving with the fluid the Sherwood number decreases and oscillates around the value 2.7 (figure 10). Peaks in that oscillation occur when the cell gets out of a turn, and troughs occur when the cell is just about to enter a turn. As the cell approaches the turn it slows (speed $\approx 0.044\,\mathrm{cm\,s^{-1}}$), and the DBL thickens in most regions around it, thus decreasing the flux of nutrients towards the cell. As the cell gets out of a turn, it accelerates (speed $\approx 0.061\,\mathrm{cm\,s^{-1}}$), and the DBL is sheared by the flow, which increases the Sherwood number.

The dimensionless Péclet number of a flow is the ratio of advective transport to diffusive transport of solutes through the fluid. Asymptotic solutions for mass transfer to spheres in steady, linear shear were derived for very large and very small Péclet numbers (see Karp-Boss *et al.* 1996 and the references therein). These asymptotic solutions provide the lower and upper bounds on expected values for $Sh$. For a cell in any pure straining motion and $Pe \ll 1$, $Sh \approx 1 + 0.36Pe^{1/2}$, and for $Pe \gg 1$, $Sh \approx 0.9Pe^{1/3}$. When both rotation and strain act and $Pe \ll 1$, $Sh \approx 1 + 0.34Pe^{1/2}$, while for $Pe\,gg\,1$, $Sh \approx 0.67Pe^{1/3}$. In our tests on a single cell $Pe \approx 40$. Lower and upper bounds for $Sh$ when $0.01 < Pe < 100$ are 1.036 and 4.18, respectively, for a pure straining motion and 1.034 and 3.11, respectively, when rotation is present. Our results fall within those bounds, since $Sh \approx 3.8$ when the cell stays at the stagnation point and $Sh \approx 2.7$ when it moves with the flow. It must be noted, however, that the relationships for $Sh$ and $Pe$ reviewed in Karp-Boss *et al.* (1996) are for spheres in steady and statistically steady shear flows, and this is not the case in our two-dimensional simulations.

### 3.2.3. *Chains of cells*

We examine effects of fluid flow on Sherwood numbers for cells in chains of different flexibilities. We start with a stiff chain ($\sigma_B^L = 10^{-4}\ \mathrm{g\,cm\,s^{-2}}$) of three cells. It is placed vertically above the centre of the domain, and the background vortical flow is imposed. The position of vortices is shifted (by $s_x = s_y = \pi/4$) every 10 s, to stay consistent with Kolmogorov time scale of the smallest velocity fluctuations of flow in the ocean. In the first few seconds the chain is pushed by the flow to the centre of the domain, a stagnation point. The flow coming symmetrically from above and below

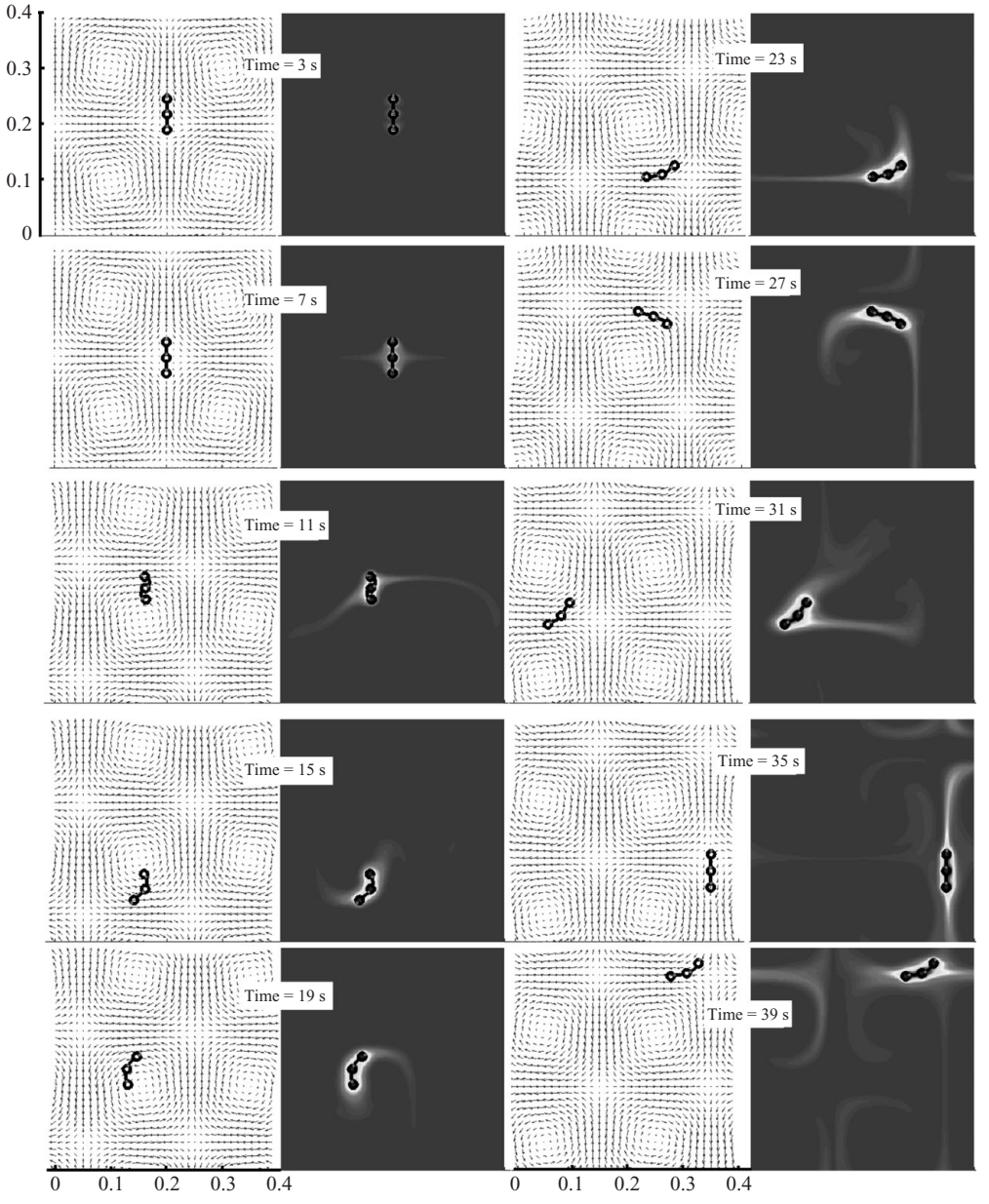


FIGURE 11. Snapshots of the nutrient concentration distribution, the position of the cell and the velocity field throughout the simulation. Stiffness of the chain is $\sigma_B^L = 10^{-4}$ g cm s$^{-2}$

keeps it in place, and since the chain is stiff it resists bending. As the positions of vortices shift, the chain begins to move with the flow and stays fairly straight through most of the simulation (figure 11).

The Sherwood number $Sh$ is large initially, since the difference between $C_\infty$ and $C_0$ that appears in the denominator (see (3.3)) is initially small. With time, $Sh$ for each cell decreases to values between 1.5 and 2 and is larger for the two end cells (cells 1 and 3). It means that cells on the exterior of the chain enjoy larger enhancement of

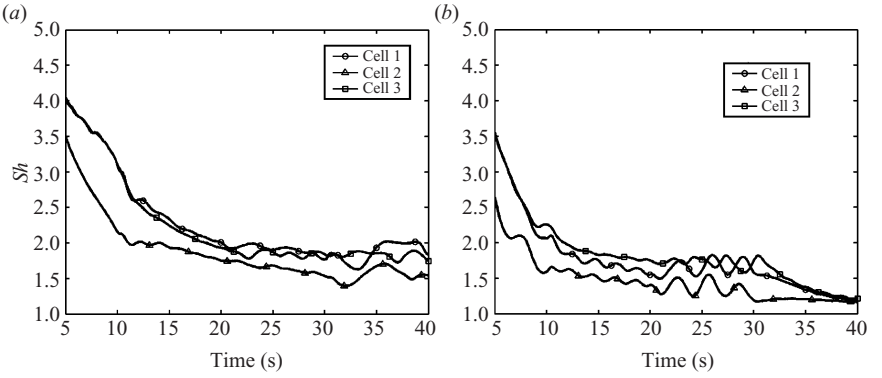


FIGURE 12. Evolution in time of the Sherwood number for each cell in (*a*) stiff and (*b*) flexible chains of three cells. The Sherwood number is initially large, since the difference between $C_\infty$ and $C_0$ is initially small.

flux due to flow than the cell in the middle (figure 12*a*). We remark that consistent results were found for chains moving in unsteady shear, presented in the previous section. When we examined nutrient uptake by cells within chains in patchy nutrient environments, throughout simulations at least one of the exterior cells often was enjoying larger nutrient uptake than the other cells in the chain.

We repeat the same experiment with a flexible chain ($\sigma_B^L = 10^{-7}$ g cm s$^{-2}$) of three cells. Just as with the stiff chain, in the first few seconds the flexible chain is pushed by the flow to the centre of the domain, a stagnation point. Since the chain is very flexible it does not resist the flow coming from above and below, and it bends easily. As the positions of vortices shift, the chain starts moving with the flow, and the cells stay close together throughout the simulation. As with previous experiments, the Sherwood number (figure 12*b*) is large initially, since the difference between $C_\infty$ and $C_0$ is initially small. As time goes by, *Sh* for each cell decreases to values between 1 and 2. Similar to the stiff chain, *Sh* for exterior cells is larger than *Sh* for the cell in the middle, as long as the cells stay in an approximately straight line, even though they are very close together (up to about $t = 30$ s). After $t = 30$ s the shape of the chain changes, from straight to triangular, and *Sh* for exterior cells decreases to approximately the same value as for the middle cell. Between the 20th and the 30th second of the simulation, *Sh* for each cell oscillates noticeably, a behaviour we also saw for a single cell. Here the reason for oscillation is similar. At those times the chain moves on the outside edge of an eddy, and the values of *Sh* change as the chain goes in and out of turns. After $t = 30$ s positions of the vortices shift, and the chain changes shape, becomes triangular and moves with the flow close to the centre of an eddy.

It is worth noticing that Sherwood numbers for cells in the stiff chain are larger than Sherwood numbers for corresponding cells in the flexible chain. Computations with chains of four or five cells also exhibited increase of Sherwood numbers with chain stiffness. Flexible chains bend, and the cells stay close together, thus decreasing the flux of nutrients to the interior parts of the squeezed or twisted chain.

## 4. Discussion

Chain formation is common among diatoms. Possible functions of chain formation are to improve nutrient supply, provide protection from grazing, alter sinking

behaviour and improve fertilization (Fryxell & Miller 1978; Sournia 1982). In the absence of data from computational, laboratory or field studies, understanding of these potential functions remains very rudimentary. Interactions of chains with the flow environment will affect any of these functions. Here we have presented a mathematical model, based on the immersed boundary method, for studying the behaviour of diatom chains in different flow regimes and the consequential delivery and uptake of nutrients. This coupled mechanical system captures the interaction of diatom cells, viscous, incompressible fluid and nutrient fields. The model examines unsteady flows and captures the flexibility of diatom chains, features that have not been included in previous models (e.g. Pahlow *et al.* 1997).

In this study we considered two types of distributions of nutrient, one in which initial nutrient concentration is uniform and another in which nutrient is introduced into the medium through point sources randomly distributed in space and time. We calculated nutrient uptake by cells and nutrient fluxes towards the cells, for solitary cells and chains of varying flexibilities. Results of numerical experiments suggest that in an oscillating flow, circular cells arranged in stiff chains consume more nutrients (per cell) than solitary cells. Pahlow *et al.* (1997) used a diffusion–advection model to compare the transport of nutrient to solitary cells and compact chains in a simple shear flow. They concluded that solitary cells will always experience increased nutrient supply compared to cells of the same shape that form chains. In their model, however, chains comprised compact cells and were modelled as prolate spheroids. Many chain-forming diatoms, however, have large gaps between cells. Our chain model of a series of spheres held by elastic, linear springs provides a realistic representation of a diatom chain. There have been no laboratory studies that compared uptake of nutrients between chains and solitary cells.

An intriguing result is the effect of chain rigidity on nutrient fluxes. Under replete conditions there is no significant difference in uptake by stiff and flexible chains, but in the patchy nutrient environment stiff chains experience an enhanced flux compared to more flexible chains of the same size and number of cells. This result may be explained by the fact that flexible chains bend more and don't resist the flow much. Stiff chains show higher resistance to flow; they bend less, maintain larger effective size and thus cover more territory and are likely to encounter a greater number of random sources. All these factors increase the nutrient concentration gradients around each cell and increase the nutrient uptake. Observations of the behaviour of stiff and flexible diatom chains in a simple shear flow qualitatively agree with the bending behaviour of flexible chains observed in our model (Karp-Boss & Jumars 1998).

This simplified two-dimensional model provides the first insights into the potential role of mechanical properties of chains and raises interesting questions regarding the evolution of diatoms. Silica frustules have the obvious benefit as a deterrent of herbivores, but here we suggest a different benefit, that of enhanced nutrient flux due to flexural stiffness. The numerical experiments further suggest that the cells on the exterior of chains experience larger enhancement of nutrient flux due to flow than the cells on the interior. This result may be explained by their smaller number of neighbours, which exposes larger parts of the cell to flow and shearing of the DBL, and also by accentuated motion, which further increases concentration gradients at the cell surface.

There is a great deal of variation in the local Sherwood number. It depends on the shape of the whole chain and the position of the cell relative to the flow. The local Sherwood number is largest in areas in which the velocity field is nearly tangential to the cell surface, since that is where the DBL is sheared most by the flow. The

local Sherwood number is lowest in areas of cell surface closest to other cells, where concentration gradients are the smallest. It is a common assumption that cells within a chain are individual units, and there is no transport of material between cells. In some species, however, cells are connected by hollow siliceous structures. It has been suggested that these structures may contain cytoplasm, so nutrients could potentially be delivered from end cells of a chain to its centre, but so far there has been no evidence for the presence of cytoplasm in linkages between cells.

In our model, diatom chains are assumed to be neutrally buoyant. However in reality they are often denser than water (generally $>1.1\,\mathrm{g\,cm^{-3}}$), largely because their frustules are made of silica. This ballasting causes them to sink at a rate of about 1 m per day (Reynolds 2006), a behaviour that can influence nutrient supply towards cells. Diatoms can also be positively buoyant, with ascent speeds up to $7–8\,\mathrm{m\,h^{-1}}$ (Moore & Villareal 1996). Thus, we want to extend our computational framework to non-neutrally buoyant immersed boundaries. To do so, we must extend the fluid solver to include a transport equation for fluid density. It can be achieved by following the work of Zhu & Peskin (2002), who studied the flapping of a filament in a flowing soap film, using an extension of the immersed boundary method that captures variable density.

Based on the analysis by Lazier & Mann (1989), we assumed that at the length scales of diatoms, the fluid flow is experienced as a simple shear flow. Their argument came from analysis of a characteristic profile of velocity in one dimension, where viscosity produces a roughly linear velocity gradient over the scale of 1 mm. Thus, in our model, we used immersed walls to create linear shear flows, but we varied direction of their movement to account for velocity fluctuations described by Kolmogorov scales. As understanding of turbulent flows grows, however, it seems that flow to which diatom cells are exposed is better described as a twisting maze of vortex worms rather than a field of steady shear and constant vorticity. Vortices are organized fluid motions rather than random fluctuations, and vortex stirring can bring reactants together in a way that random fluctuations cannot (Crimaldi, Hartford & Weiss 2006). Therefore, to examine effects of vorticity gradients and time-varying vorticity on phytoplankton cells, we plan to incorporate in our model various vorticity fields, such as Burgers vortex (Davidson 2004). However, since in two dimensions vortex stretching cannot occur and vorticity is limited to the axis orthogonal to the two dimensions, we must follow the presented model into three dimensions. The behaviour of chains in three dimensions is obviously more complex than that in two dimensions. They can rotate in more than one dimension. There are gaps between cells through which both fluid and nutrient can flow, which in the two-dimensional model are limited. This kind of flow will have effect on nutrient transport towards the cells, since shearing of the DBL may occur also between cells, which in turn will affect concentration gradients and the Sherwood number.

Numerical computations of the sort begun here appear to be an efficient way to identify phenomena of potential interest that can then be pursued experimentally. Production of vortices that have diameters of a few centimetre in the laboratory is feasible for experimental purposes once testable alternative hypotheses, suggested by numerical results, have been framed. Hunting phenomena and identifying mechanisms in laboratory or field observations would be a much more daunting task.

This work of M. Musielak and L. Fauci was partially supported by NSF OCE-0724598, and the work of P. A. Jumars and L. Karp-Boss was partially supported by NSF OCE-0724744.

## REFERENCES


Almqvist, N., Delamo, Y., Smith, B. L., Thomson, N. H., Bartholdson, A., Lal, R., Brzezinski, M. & Hansma, P. K. 2001 Micromechanical and structural properties of a pennate diatom investigated by atomic force microscopy. *J. Microsc.* **202** (3), 518–532.

Blackburn, N., Azam, F. & Hagstrom, A. 1997 Spatially explicit simulations of microbial food web. *Limnol. Oceanogr.* **42** (4), 613–622.

Crimaldi, J. P., Hartford, J. R. & Weiss, J. B. 2006 Reaction enhancement of point sources due to vortex stirring. *Phys. Rev.* E **74**, 016307.1-016307.4.

Davidson, P. A. 2004 *Turbulence: An Introduction for Scientists and Engineers*. Oxford University Press.

Dillon, R., Fauci, L., Fogelson, A. & Gaver, D. 1996 modelling biofilm processes using the immersed boundary method. *J. Comput. Phys.* **129**, 57.

Fauci, L. & McDonald, A. 1994 Sperm motility in the presence of boundaries. *Bull. Math. Biol.* **57**, 679.

Fryxell, G. A. & Miller, W. I. 1978 Chain-forming diatoms: three araphid species. *Bacillaria* **1**, 113–136.

Jeffery, G. B. 1922 The motion of ellipsoidal particles immersed in a viscous fluid. *Proc. R. Soc. Lond.* A **102** (715), 161–179.

Jumars, P. A., Boss, E., Trowbridge, J. H. & Karp-Boss, L. 2009 Turbulence–plankton interactions: a new cartoon. *Mar. Ecol.* **30**, 133–150.

Karp-Boss, L., Boss, E. & Jumars, P. A. 1996 Nutrient fluxes to planktonic osmotrophs in the presence of fluid motion. *Oceanogr. Mar. Biol.* **34**, 71–107.

Karp-Boss, L. & Jumars, P. A. 1998 Motion of diatom chains in steady shear flow. *Limnol. Oceanogr.* **43** (8), 1767–1773.

Kim, J. & Moin, P. 1985 Application of a fractional-step method to incompressible Navier–Stokes equations. *J. Comput. Phys.* **59**, 308–323.

Kiørboe, T., Ploug, H. & Thygesen, U. H. 2001 Fluid motion and solute distribution around sinking aggregates. Part 1. Small-scale fluxes and heterogeneity of nutrients in the pelagic environment. *Mar. Ecol. Prog. Ser.* **211**, 1–13.

Kleis, S. J. & Rivera-Solorio, I. 2003 Time scales for unsteady mass transfer from a sphere at low-finite reynolds numbers. *J. Heat Transfer* **125** (4), 716–723.

Lazier, J. R. N. & Mann, K. H. 1989 Turbulence and the diffusive layers around small organisms. *Deep-Sea Res.* **36** (11), 1721–1733.

Li, T., Deen, N. G. & Kuipers, J. A. M. 2005 Numerical investigation of hydrodynamics and mass transfer for in-line fibre arrays in laminar crossflow at low Reynolds numbers. *Chem. Engng Sci.* **60**, 1837–1847.

Martin-Jézéquel, V., Hildebrand, M. & Brzezinski, M. A. 2000 Silicon metabolism in diatoms: implications for growth. *J. Phycol.* **36**, 821–840.

Mittal, R. & Iaccarino, G. 2005 Immersed boundary methods. *Annu. Rev. Fluid Mech.* **37**, 239–261.

Moore, J. K. & Villareal, T. A. 1996 Size-ascent rate relationships in positively buoyant marine diatoms. *Limnol. Oceanogr.* **41** (7), 1514–1520.

Munk, W. H. & Riley, G. A. 1952 Absorption of nutrients by aquatic plants. *J. Mar. Res.* **11**, 215–40.

Musielak, M. M. 2007 A computational model of nutrient transport and acquisition by diatom chains in a moving fluid. PhD thesis, Tulane University, New Orleans, LA, USA.

Paasche, E. 1973 Silicon and the ecology of marine plankton diatoms. Part 2. Silicate-uptake kinetics in five diatom species. *Mar. Biol.* **19**, 262.

Pahlow, M., Riebesell, U. & Wolf-Gladrow, D. A. 1997 Impact of cell shape and chain formation on nutrient acquisition by marine diatoms. *Limnol. Oceanogr.* **42** (8), 1660–1672.

Peskin, C. S. 2002 The immersed boundary method. *Acta Num.* **11**, 479–517. Published online by Cambridge University Press, 15 July 2003.

Purcell, E. M. 1977 Life at low Reynolds number. *Am. J. Phys.* **45**, 3–11.

Reynolds, C. S. 2006 *The Ecology of Phytoplankton*. Cambridge University Press.

Round, F. E., Crawford, R. M. & Mann, D. G. 1990 *The Diatoms: Biology and Morphology of the Genera*. Cambridge University Press.

Shimeta, J. S., Jumars, P. A. & Lessard, E. J. 1995 Influences of turbulence on suspension feeding by planktonic protozoa: experiments in laminar shear field. *Limnol. Oceanogr.* **40**, 845–859.

Short, M., Solari, C., Ganguly, S., Powers, T., Kessler, J. & Goldstein, R. 2006 Flows driven by flagella of multicellular organisms enhance long-range molecular transport. *Proc. Natl Acad. Sci. USA* **103**, 8315–8319.

Solari, C. A., Ganguly, S., Kessler, J. O., Michod, R. E. & Goldstein, R. E. 2006 Multicellularity and the functional interdependence of motility and molecular transport. *Proc. Natl Acad. Sci. USA* **103**, 1353–1358.

Sournia, A. 1982 Form and function in marine phytoplankton. *Biol. Rev.* **57**, 347–394.

Tada, S. & Tarbell, J. M. 2004 Internal elastic lamina affects the distribution of macromolecules in the arterial wall: a computational study. *Am. J.Physiol: Heart Circ. Physiol.* **287**, H905–H913.

Tennekes, H. & Lumley, J. L. 1972 *A First Course in Turbulence*. MIT Press.

Thamatrakoln, K. & Hildebrand, M. 2008 Silicon uptake in diatoms revisited: a model for saturable and nonsaturable uptake kinetics and the role of silicon transporters. *Plant Physiol.* **146**, 1397–1407.

Thorpe, S. A. 2007 *An Introduction to Ocean Turbulence*. Cambridge University Press.

Tomas, C. R. (Ed.) 1997 *Identifying Marine Phytoplankton*. Academic Press.

Werner, D. (Ed.) 1977 *The Biology of Diatoms*. *Botanical Monographs*, vol. 13. University of California Press.

Zhu, L. & Peskin, C. S. 2002 Simulation of a flapping flexible filament in a flowing soap film by the immersed boundary method. *J. Comput. Phys.* **179**, 452–468.